MATERIALS CHEMISTRY FRONTIERS

RESEARCH ARTICLE

View Article Online
View Journal | View Issue

Cite this: *Mater. Chem. Front.*, 2023, **7**, 2411

Compositionally tuned hybridization of n-type Ag^0 : Ag_2Se under ambient conditions towards excellent thermoelectric properties at room temperature†

Si Yin Tee, *[a] Daniel Ponsford,[abc] Xian Yi Tan,[ad] Xiaobai Wang,[a] Chee Leng Lay,[a] Coryl Jing Jun Lee,[a] Xi Ping Ni,[a] Debbie Hwee Leng Seng,[a] Warintorn Thitsartarn,[a] Guijian Guan [e] and Ming-Yong Han *[ae]

Received 2nd February 2023,
Accepted 17th March 2023

DOI: 10.1039/d3qm00123g

rsc.li/frontiers-materials

It is important to tune the thermoelectric properties of n-type thermoelectric materials, orthorhombic Ag_2Se by nanoscale hybridization apart from conventional alloying or ion-doping approaches. In this work, we report the thermoelectric performance of a series of n-type Ag^0 : Ag_2Se materials prepared through a surfactant-free, aqueous solution-based approach under ambient conditions. This strategy enables fine control over phases and compositions through nanoscale hybridization using silver nanoparticles for the first time, yet remains applicable to large-scale production methods. By prolonging reaction times, the synthetic process is carefully developed/optimized to adjust the excess of the Ag^0 phase, in order to enhance the thermoelectric properties. Hybridization of Ag^0 and Ag_2Se with increasing amounts of Ag^0 (1.96%, 4.31%, 6.10%, 15.97%, 45.80% and 50.86% Ag^0) results in not only increased electrical conductivities but also decreased Seebeck coefficients. The optimal excess of Ag^0 is determined to be 1.96% after 7 days of reaction, with a high *ZT* value of near unity at 333 K. The *ZT* values realized in this study exceed those hitherto reported for β-Ag_2Se synthesized *via* wet chemistry methods at room temperature.

1. Introduction

Thermoelectric materials enable the direct conversion of thermal to electric energy, and as such have received considerable attention as a source of renewable energy. The most significant thermoelectric advances have been achieved in power generation applications using cubic semiconductors, particularly PbTe,[1] SnTe,[2] and GeTe[3] due to their outstanding thermoelectric performance at mid-temperatures (500–800 K). On the other hand, there has been noticeably less attention devoted to the study of near-room-temperature thermoelectric materials, although statistical data reveal that low-grade waste heat at temperatures <100 °C accounts for $\sim$63% of total waste heat worldwide.[4–6] Recently, orthorhombic Ag_2Se has attracted much interest for near-room-temperature thermoelectric applications, owing to its outstanding electrical conductivity and glass-like thermal conductivity.[7,8] As such, Ag_2Se and hybridized Ag_2Se have also shown great potential for use in thermoelectric cooling[9] and driving wearable electronics/sensors.[8,10,11]

In order to optimize the thermoelectric performance of orthorhombic Ag_2Se, it is vital to understand the correlation between its composition, structure, and transport properties. Beyond the phase transition from orthorhombic to cubic phase, Ag_2Se possesses superionic properties due to the mobility of Ag^+ ions within a rigid lattice of Se^{2-} at high temperatures above 407 K.[12] A variety of methods have been successfully developed for the preparation of Ag_2Se thermoelectric materials, including high-temperature solid-state reactions,[7,13] room-temperature grinding,[14] high-energy mechanical milling,[15,16] and pulsed hybrid reactive magnetron sputtering techniques.[17] In comparison, solution-based approaches are relatively less investigated for the synthesis of Ag_2Se, though widely used for generating CdSe, ZnSe and $Cu_{2-x}Se$ compounds,[18–21] as these methods offer the unique advantage of excellent control over

[a] *Institute of Materials Research and Engineering (IMRE), Agency for Science, Technology and Research (A*STAR), 2 Fusionopolis Way, Innovis #08-03, Singapore 138634, Republic of Singapore. E-mail: teesyi@imre.a-star.edu.sg, my-han@imre.a-star.edu.sg*
[b] *Department of Chemistry, University College London, WC1H 0AJ, UK*
[c] *Institute for Materials Discovery, University College London, WC1E 7JE, UK*
[d] *Department of Materials Science and Engineering, Nanyang Technological University, 639798, Singapore*
[e] *Institute of Molecular Plus, Tianjin University, Tianjin 300072, China. E-mail: han_mingyong@tju.edu.cn*

† Electronic supplementary information (ESI) available. See DOI: https://doi.org/10.1039/d3qm00123g

material stoichiometry with high production throughputs under ambient conditions. The colloidal synthesis of Ag_2Se is typically performed in an organic phase at elevated temperatures, which involves the use of organic surfactants and/or solvents.[22] As a result, the synthesized chalcogenide particles are coated with organic species, which adversely impact the electronic transport of charge carriers. Commonly, a complex ligand exchange process is needed to remove organic surfactants.[12,23] Thus, it is highly desirable to design a scalable process for the synthesis of Ag_2Se with high thermoelectric performance under aqueous conditions in the absence of ligands or surfactants.

The current aqueous synthetic methods have demonstrated effective control over phase and compositions of alloyed/doped Ag_2Se with other metals or chalcogens, which is achieved by altering reaction parameters such as pH.[24] To gain more insight into the high thermoelectric performance of the Ag_2Se system, hybridized Ag_2Se with Ag^0 has been systematically prepared in aqueous solution at room temperature. This technique does not require heating, multiple processing treatments and expensive or toxic solvents. The stoichiometry of Ag and Se was finely controlled by modulating the oxidation states of Ag and Se in the reaction medium, producing a series of Ag^0:Ag_2Se (Ag^0 excess at 50.86%, 45.80%, 15.97%, 6.10%, 4.31% and 1.96%) with enhanced thermoelectric properties. The optimal excessive Ag^0 was determined to be 1.96% after 7 days of reaction and a high *ZT* of near unity at 333 K was achieved. This result demonstrates the potential of $Ag^0:Ag_2Se$ to serve as an alternative to state-of-the-art n-type Bi_2Te_3.[25] Bi_2Te_3 is currently the only commercially available thermoelectric material for use in room-temperature applications, although its usage is limited by the scarce availability and toxicity of tellurium. As a result, alternatives to Bi_2Te_3, such as $Ag^0:Ag_2Se$, are highly preferable. This research provides a new method to improve the thermoelectric properties by tuning the carrier concentration through controlled hybridization, without changing the intrinsic properties of Ag_2Se. This method is unlike typical doping techniques that form alloys, which are limited due to the low solubility of dopants in the alloys.

2. Results and discussion

2.1 Compositionally tuned hybridization and characterization of $Ag^0:Ag_2Se$ hybrids

The aqueous synthesis of hybridized $Ag^0:Ag_2Se$ at room temperature is demonstrated as follows (Fig. 1A). First, $NaBH_4$ reduced SeO_3^{2-} to form colourless Se^{2-} under argon protection. An aqueous solution of $AgNO_3$ was then injected slowly, forming a black precipitate. After reaction for 2 h, the resulting black powder was characterized by XRD (Fig. 1B) and SEM EDX (Fig. 1D and Fig. S1, ESI†) to confirm the formation of a mixture of orthorhombic Ag_2Se (JCPDS 24-1041) and cubic Ag^0 (JCPDS 01-071-4613). The as-synthesized $Ag^0:Ag_2Se$ hybrids were obtained after reaction for 2, 24, 48, 72, 120 and 168 h (denoted as days 0, 1, 2, 3, 5 and 7 respectively), possessing the respective molar ratios (Ag:Se) of 4.07, 3.69, 2.38, 2.13, 2.09 and 2.04

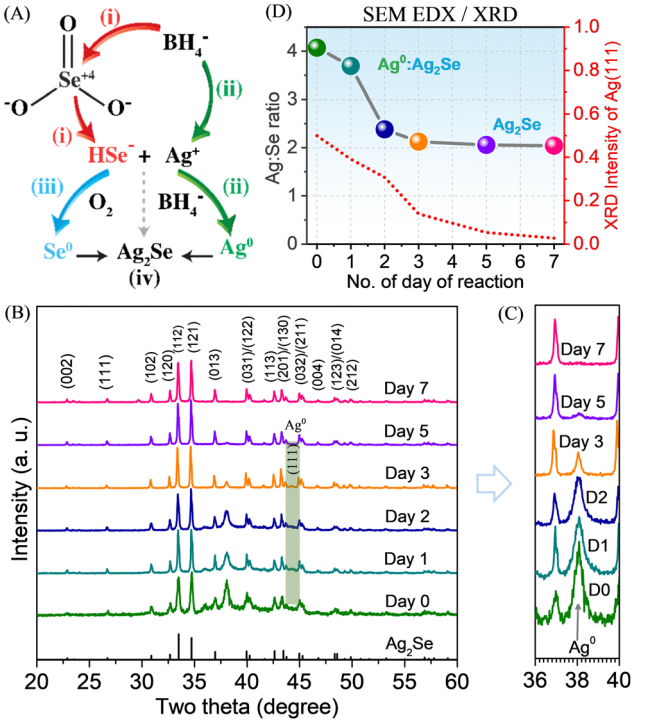

Fig. 1 (A) Schematic synthesis of $Ag^0:Ag_2Se$ hybrids at room temperature under aqueous conditions, with different molar ratios of Ag:Se. (B) Whole and (C) partial XRD patterns of the as-synthesized $Ag^0:Ag_2Se$ powders obtained after reaction for 0, 1, 2, 3, 5 and 7 days (denoted as day 0, 1, 2, 3, 5 and 7), corresponding to excessive Ag^0 at 50.86%, 45.80%, 15.97%, 6.10%, 4.31% and 1.96%, respectively. (D) EDX-determined compositions and XRD intensities of Ag^0 for the as-synthesized $Ag^0:Ag_2Se$ powders as a function of reaction time.

(Ag:Se = 2 for phase-pure Ag_2Se in Fig. S1, ESI†). The molar ratios correspond to excessive Ag^0 at 50.86%, 45.80%, 15.97%, 6.10%, 4.31% and 1.96% respectively, in agreement with the reduced XRD peaks at 38.1° in Fig. 1D from the (111) plane of Ag^0. The presence of excessive Ag^0 was confirmed by the prominent diffraction peak after 0, 1, 2, and 3 days of reaction (Fig. 1B and C). The XRD peak was comparatively less distinguishable after 5 days of reaction (4.31% $Ag^0:Ag_2Se$), and almost disappeared after 7 days of reaction (1.96% $Ag^0:Ag_2Se$).

As observed in the SEM and TEM (inset) images (Fig. S2A, ESI†), 1.96% $Ag^0:Ag_2Se$ particles have a granular structure of ~200–500 nm in size. Thermal analysis in the DSC thermogram (Fig. S2B, ESI†) reveals the appearance of an endothermic peak at 407 K and an exothermal peak at 382 K during the heating and cooling processes, respectively. The reversible phase transition was also demonstrated by temperature-dependent XRD analysis. A structural change from orthorhombic (β-Ag_2Se) to cubic phase (α-Ag_2Se) upon heating was observed, as well as a structural conversion back to β phase again upon cooling (Fig. 2). The variable temperature XRD analysis clearly shows the structural transition from the low-temperature orthorhombic phase to the high-temperature cubic phase.

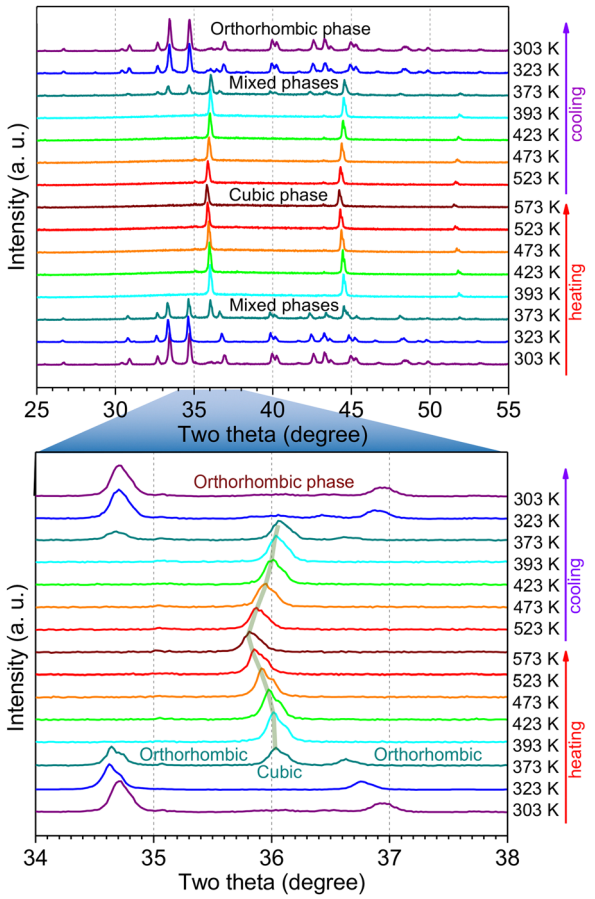

Fig. 2 Temperature-dependent XRD patterns of the as-prepared 1.96% Ag^0 : Ag_2Se powder (after 7 days of reaction) by *in situ* XRD measurements upon heating from 303, 323, 373, 393, 423, 473, 523 to 573 K, and cooling from 573, 523, 473, 423, 393, 373, 323 to 303 K.

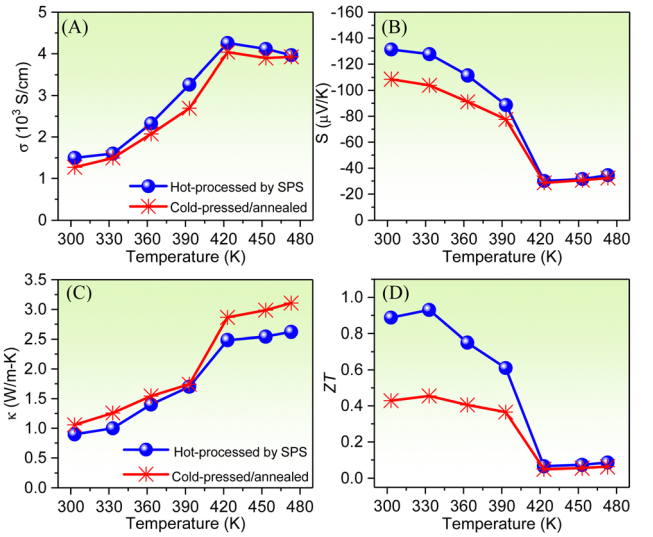

Fig. 3 Temperature dependence of (A) electrical conductivity, (B) Seebeck conductivity, (C) thermal conductivity, and (D) *ZT* values of 1.96% Ag^0 : Ag_2Se pellets after being cold-pressed/annealed at 200 °C (red) and hot-pressed at 200 °C by SPS (blue).

Initially, only an orthorhombic phase was observed at 303 K. At an elevated temperature of 373 K (100 °C), mixed orthorhombic and cubic phases were detected, indicating the partial phase change from orthorhombic to cubic phase. A complete phase change occurred at a higher temperature of 393 K, although this is significantly lower than the starting point of the sharp peak for heat flow at 407 K in the DSC thermogram (Fig. S2, ESI†), indicating the phase change from orthorhombic to cubic phase occurs at a relatively lower temperature. In the cubic structure, two theta degree shifted from 35.81 to 36.27° with a *d*-spacing increase from 0.2492 to 0.2507 Å when the temperature was increased from 393 K to 573 K. With the decrease of temperature from 573 K to 393 K, the two theta degree shifted to 36.06° with a decrease in *d*-spacing to 0.2490 Å.

2.2 Thermoelectric properties of cold-pressed/annealed *vs.* hot-pressed pellets of 1.96% Ag^0 : Ag_2Se hybrids

Surfactant-free powder of 1.96% Ag^0 : Ag_2Se in several grams was prepared by our solution-based one-pot approach and consolidated into pellets for thermoelectric studies. As shown in Fig. S3 (ESI†), XRD patterns of Ag^0 : Ag_2Se in different forms were collected for (i) the as-prepared powder, (ii) the cold-pressed pellet, (iii) the cold-pressed pellet after annealing at 200 °C, and (iv) the hot-pressed pellet by SPS at 200 °C. All the processed samples had a low-temperature orthorhombic phase of Ag_2Se (JCPDS no. 24-1041). The consolidated pellets were prepared at 473 K (200 °C), far above the phase transition temperature at 407 K (134 °C) from the orthorhombic to cubic phase.

Thermoelectric properties of the cold-pressed pellet of 1.96% Ag^0 : Ag_2Se were investigated after annealing at 200 °C (Fig. 3). Temperature-dependent electrical conductivity of the pellet (Fig. 3A) clearly reveals the transition from semiconducting to metallic behaviour, as indicated by a gradual increase of the electrical conductivity with increasing temperature from 1269.78 S cm^{-1} (303 K) to 2695.98 S cm^{-1} (393 K), and then a drastic increase to 4039.25 S cm^{-1} (423 K), which was followed by a slight decrease to 3924.86 S cm^{-1} (473 K). The temperature-dependent Seebeck coefficient (Fig. 3B) was negative in a broad range of temperature (303–473 K), which is indicative of the n-type semiconductor characteristics of solution-synthesized Ag^0 : Ag_2Se. The Seebeck coefficient decreased gradually with increasing temperature from −108.92 μV K^{-1} (303 K) to −77.52 μV K^{-1} (393 K), followed by a drastic decrease to −28.70 μV K^{-1} (423 K) and −32.34 μV K^{-1} (473 K). Temperature-dependent thermal conductivity was also measured (Fig. 3C). An initial increase from 1.05 W m^{-1} K^{-1} (303 K) to 1.74 W m^{-1} K^{-1} (393 K) was observed, and then a drastic increase to 2.87 W m^{-1} K^{-1} (423 K) followed by a slight increase to 3.11 W m^{-1} K^{-1} (473 K). Overall, the thermal conductivity shows a similar trend of the electrical conductivity but an opposite trend to that of the Seebeck coefficient between 303 and 473 K.

The thermoelectric properties of the hot-pressed pellet by SPS were investigated as well (Fig. 3), showing similar trends to

the cold-pressed/annealed pellets. A higher electrical conductivity and Seebeck coefficient (Fig. 3A) but a lower thermal conductivity (Fig. 3C) were measured at each temperature for the hot-pressed pellet compared to the cold-pressed/annealed pellet. Through a closer examination with SEM/XRD, the cold-pressing process is carried out by sequentially pressing at room temperature and sintering (1 atm) at 200 °C, resulting in inefficient densification of the pellet with a grain size of ~90 nm, as estimated by the XRD Scherrer equation. In comparison, the hot-pressing process by SPS proceeds by concurrently pressing and sintering (under pressure) at 200 °C, resulting in efficient densification to achieve a finer-grained dense structure[26] with a grain size of ~40 nm, as estimated by the XRD Scherrer equation (Fig. S4, ESI†). The smaller grain size with shorter phonon mean free path increases the scattering of phonons at grain boundaries to restrict the thermal conductivity.[27,28] Collectively, the SPS-processed Ag_2Se generated a high *ZT* of around unity at 333 K (Fig. 3D), which is more than double that of the cold-pressed/annealed pellet, suggesting that the densification process strongly influences the resulting thermoelectric properties of the material.

2.3 Thermoelectric properties of hot-pressed pellets of 1.96% *vs.* 4.31% $Ag^0:Ag_2Se$ hybrids

The temperature-dependent electrical conductivity of the 4.31% $Ag^0:Ag_2Se$ pellet was obtained in comparison with the 1.96% $Ag^0:Ag_2Se$ pellet after hot-processing by SPS (Fig. 4). The 1.96% $Ag^0:Ag_2Se$ pellet exhibited an electrical conductivity of 1524.74 S cm^{-1} (303 K), which rapidly rose to 4259.62 S cm^{-1} (423 K) and remained almost constant in the 423–473 K range (Fig. 4A). The abrupt increase in electrical conductivity indicates a surge disordering in the arrangement of Ag atoms in the rigid body-centric network of selenium, resulting in superionic conductivity. On the other hand, the 4.31% $Ag^0:Ag_2Se$ pellet showed relatively higher electrical conductivity at temperatures below 393 K such as 1762.70 S cm^{-1} at 303 K and a similar one of 4254.16 S cm^{-1} at 423 K, arising from the higher content of Ag^0 than the 1.96% $Ag^0:Ag_2Se$ pellet. The increased excess of Ag^0 was also accompanied by a significant drop in Seebeck coefficient of −112.46 μV K^{-1} (4.31% $Ag^0:Ag_2Se$) compared to −131.22 (1.96% $Ag^0:Ag_2Se$) at room temperature (Fig. 4B). The difference in Seebeck coefficient was less obvious with increasing temperature, presenting the values of approximately −30 μV K^{-1} (423 K) and −35 μV K^{-1} (473 k) for the 1.96% $Ag^0:Ag_2Se$.

The temperature-dependent thermal conductivity of 4.31% $Ag^0:Ag_2Se$ was also measured (Fig. 4C), showing a similar trend as 1.96% $Ag^0:Ag_2Se$. The 1.96% $Ag^0:Ag_2Se$ pellet showed an initial increase from 0.90 W m^{-1} K^{-1} (303 K) to 1.64 W m^{-1} K^{-1} (393 K) and then a drastic increase to 2.48 W m^{-1} K^{-1} (423 K) and 2.62 W m^{-1} K^{-1} (473 K). With a higher content of Ag^0, the 4.31% $Ag^0:Ag_2Se$ pellet clearly exhibited higher thermal conductivities of 0.98 W m^{-1} K^{-1} (303 K), 1.76 W m^{-1} K^{-1} (393 K), 2.60 W m^{-1} K^{-1} (423 K) and 2.71 W m^{-1} K^{-1} (473 K). Furthermore, the temperature-dependent thermal conductivity of the $Ag^0:Ag_2Se$ pellet showed a similar trend of electrical conductivity (Fig. 4A).

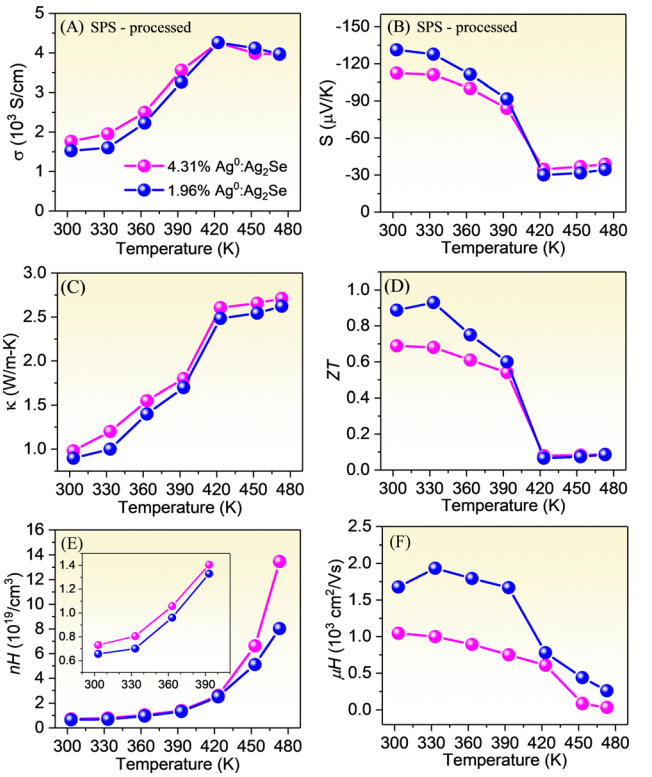

Fig. 4 Temperature dependence of (A) electrical conductivity, (B) Seebeck coefficient, (C) thermal conductivity, (D) *ZT* value, (E) carrier concentration, and (F) carrier mobility of the 1.96% $Ag^0:Ag_2Se$ pellet in comparison with the 4.31% $Ag^0:Ag_2Se$ pellet, which were both hot-processed by SPS at 200 °C.

Temperature-dependent *ZT* for 1.96% and 4.31% $Ag^0:Ag_2Se$ pellets is presented in Fig. 4D as a function of temperature. The *ZT* value of the 4.31% $Ag^0:Ag_2Se$ pellet reached 0.69 (303 K) and gradually decreased to 0.56 (393 K), followed by a drastic drop to 0.08 (423–473 K). The 1.96% $Ag^0:Ag_2Se$ pellet showed an increase in *ZT* from 0.89 (303 K) to 0.94 (333 K) and then a gradual drop to 0.62 with a further increase in temperature at 393 K. Beyond this temperature, a rapid drop in *ZT* to 0.07 was observed due to the phase transition to the cubic phase. Above the phase transition temperature, *ZT* for 1.96% and 4.31% $Ag^0:Ag_2Se$ remained almost constant with increasing temperature up to 473 K. In comparison, the thermoelectric performance of the 4.31% $Ag^0:Ag_2Se$ pellet was markedly lower than that of the 1.96% $Ag^0:Ag_2Se$ pellet.

The maximum *ZT* value of the 1.96% $Ag^0:Ag_2Se$ pellet was 0.94 at 333 K, which represents a 134% enhancement compared to the 4.31% $Ag^0:Ag_2Se$ pellet. This increase in *ZT* value mainly originates from the lower thermal conductivity and higher power factor, as well as the optimized transport properties (*i.e.*, electrical conductivity, carrier concentration and carrier mobility) and Seebeck coefficient due to the composition tuning of Ag^0 in Ag_2Se. In comparison to stoichiometric Ag_2Se, the inclusion of Ag^0 in Ag_2Se is advantageous to boost the electrical transport properties and improve the overall thermoelectric performance, particularly at room temperature.[24]

At room temperature, the maximum *ZT* value (0.89 at 303 K) for the $Ag^0:Ag_2Se$ hybrid (hybridized rather than doped) is

higher than the corresponding values for Ag_2Se synthesized at room temperature in aqueous solution (0.45 at 323 K[29] and 0.80 at 303 K[24]), Ag_2Se synthesized at high temperature in organic solvent (0.55 at 300 K),[30] and Ag_2Se synthesized *via* a hydrothermal process (0.6 at 300 K)[31] and solvothermal process in organic solvent (0.7 at 317 K).[32] The increased *ZT* for the Ag^0 : Ag_2Se hybrids is attributed to the incorporation of a small percentage of Ag^0 in Ag_2Se. Moreover, the excellent stability achieves reproducible thermoelectric properties after 5 cycles of consecutive measurements (Fig. S5, ESI†).

2.4 Carrier concentration and mobility of hot-pressed pellets of 1.96% and 4.31% Ag^0 : Ag_2Se hybrids

In order to understand the change in electrical conductivity and Seebeck coefficient with increasing temperature, temperature-dependent carrier concentrations of the 1.96 and 4.31% Ag^0 : Ag_2Se pellets were measured (Fig. 4E). At lower temperature, there was a continuous increase in the carrier concentration of 1.96% Ag^0 : Ag_2Se from 6.56×10^{18} cm^{-3} (303 K) to 1.33×10^{19} cm^{-3} (393 K) with increasing temperature. Beyond the transition temperature (393 K) from the semiconducting orthorhombic phase to the superionic cubic phase of Ag_2Se (Ag^+ ions become mobile within a rigid lattice of Se^{2-}), the carrier concentration increased significantly to 8.03×10^{19} cm^{-3} (473 K). With an increase of Ag^0 content to 4.31%, higher carrier concentrations were observed from 7.31×10^{18} cm^{-3} (303 K) to 1.45×10^{19} cm^{-3} (393 K) and 1.35×10^{20} cm^{-3} (473 K). This is mainly because the Ag can inject electrons into the conduction band of Ag_2Se to increase the carrier concentration. As the Seebeck coefficient is inversely proportional to the 2/3 power of the carrier concentration (n) according to $S \propto Tn^{2/3}$,[33] the tendency of change of the Seebeck coefficient with temperature is opposite to that of the carrier concentration with temperature (T) as shown in Fig. 4B.

Temperature-dependent carrier mobility of Ag^0 : Ag_2Se pellets decreased monotonically with increasing temperature (Fig. 4F), in contrast to the change/increase in the carrier concentration. This tendency was similarly reported in the literature regarding Ag_2Se.[17,34] The carrier mobility measured for the 4.31% Ag^0 : Ag_2Se pellet was systematically lower than that of the 1.96% Ag^0 : Ag_2Se pellet. This arises directly from the higher Ag^0 content, which has a lower carrier mobility of 50 $cm^2\ V^{-1}\ s^{-1}$ at 303 K compared with $\sim 10^3$ $cm^2\ V^{-1}\ s^{-1}$ for Ag_2Se. In addition, Ag nanoparticles may scatter electrons to further decrease the carrier mobility.[33] At 303 K, both the hybridized samples (4.31% and 1.96% Ag^0 : Ag_2Se) demonstrated high carrier mobilities of 1045.21 $cm^2\ V^{-1}\ s^{-1}$ and 1677.35 $cm^2\ V^{-1}\ s^{-1}$, respectively. The lower carrier mobility of 4.31% Ag^0 : Ag_2Se relates to the higher carrier concentration, *i.e.*, higher electrical conductivity due to the incorporation of more Ag^0 in Ag_2Se.

2.5 Preparative mechanism for revealing structural control in the hybridization of Ag^0 : Ag_2Se

It is important to tune the interior composition and components of Ag^0 : Ag_2Se, as this substantially influences the thermoelectric properties of the material. In order to produce the hybridized Ag^0 : Ag_2Se in this work (Fig. 1A), Na_2SeO_3 was first reduced by $NaBH_4$ under an argon flow with a Schlenk line to form a colourless solution of Se^{2-} at pH 13.32, according to the following exothermic reaction: $3NaBH_4 + 4Na_2SeO_3 \rightarrow 4Na_2Se + 3NaBO_2 + 6H_2O$. An aqueous solution of $AgNO_3$ (pH 4.12) was then added to reduce the pH to 9.41 (significantly lower than the pKa of HSe^- at pH 11.0) after the reaction with Se^{2-} to form HSe^-. Meanwhile, Ag^+ was reduced by $NaBH_4$ to form a black Ag precipitate, according to the following reaction: $2AgNO_3 + 4NaBH_4 + 7H_2O \rightarrow 2Ag^0 + Na_2B_4O_7 + 2NaNO_3 + 15H_2$. Rather than forming Ag_2Se *via* $2Ag^+ + HSe^- \rightarrow Ag_2Se + H^+$ at pH less than the pKa of HSe^-, small Ag nanoparticles of $\sim$20 nm (a FESEM image in Fig. S6A, ESI†) were the majority product upon the reduction of $AgNO_3$ by $NaBH_4$ for 2 min (very early stage), which quickly agglomerated in the absence of stabilizer. The EDX spectrum of the as-obtained powder gave a ratio of 93.81% Ag^0 : Ag_2Se (Fig. S6B, ESI†). The dominant existence of Ag^0 was confirmed by XRD characterization (Fig. S6C, ESI†), showing the cubic Ag^0 phase (JCPDS # 01-071-4613) with a major peak at 38.1° from the (111) plane of metallic Ag particles.

Under continuous argon purging, the supernatant remained colourless with increasing time (black Ag precipitate). When argon purging was halted after 2 min of reaction, oxygen was slowly introduced into the three-neck flask and diffused into the above colourless solution. Once exposed to oxygen, a brick-red solution of Se^0 formed quickly (Fig. S4D, ESI†) *via* an oxidative reaction of HSe^- with dissolved O_2 *via* $2HSe^- + O_2 \rightarrow 2Se^0 + 2OH^-$. After 2 h, 50.86% Ag^0 : Ag_2Se was obtained *via* the reaction of Se^0 on the surface of Ag^0 nanoparticles to form Ag_2Se ($Ag^0 + 2Se^0 \rightarrow Ag_2Se$). Longer durations are required for further reaction under the surface layer (due to slow diffusion) to control the ratio of Ag^0/Ag_2Se. With increasing reaction times of 1, 2, 3, 5 to 7 days, hybridized Ag^0 : Ag_2Se samples with a reduced amount of Ag^0 at 50.86%, 45.80%, 15.97%, 6.10%, 4.31% and 1.96% respectively were obtained (Fig. S7, ESI†).

2.6 Compositionally tuned hybrids for revealing thermoelectric properties

The amount of Ag^0 in Ag^0 : Ag_2Se hybrids was varied over a wide range of compositions in this research. Varying the duration of time (1, 3, 5 and 7 days) following the initial aqueous synthesis provided an effective strategy to investigate, tune and understand the thermoelectric properties of Ag^0 : Ag_2Se after hot-processing by SPS. The temperature-dependent electrical conductivity of 45.80% Ag^0 : Ag_2Se prepared by reaction for 1 day (Fig. 5A) was measured as 14247.26 S cm^{-1} at 303 K and further increased to 19430.84 S cm^{-1} at 423 K. When the reaction time was prolonged, more Ag_2Se was converted from Ag^0, resulting in a drastic decrease in electrical conductivity by $\sim$600% at 303 K for all the Ag^0 : Ag_2Se samples including 6.10%, 4.31%, and 1.96% Ag^0 from 3, 5 and 7 days of reaction, respectively.

The 45.80% Ag^0 : Ag_2Se had a significantly higher electrical conductivity than the rest of the Ag^0 : Ag_2Se samples, which is related to its augmented carrier concentration (1.47×10^{21} cm^{-3} at

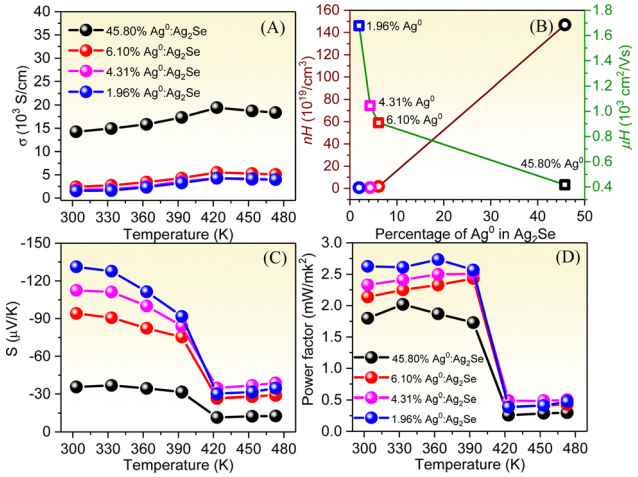

Fig. 5 Temperature dependence of (A) electrical conductivity, (B) carrier concentration (circle)/carrier mobility (square), (C) Seebeck conductivity, and (D) power factors of the hot-pressed pellets of 45.80%, 6.10%, 4.31%, and 1.96% $Ag^0:Ag_2Se$, synthesized after reactions for 1, 3, 5, and 7 days.

303 K *vs.* 1.69×10^{19} cm^{-3}, 0.73×10^{19} cm^{-3} and 0.66×10^{19} cm^{-3}) due to hybridization with more Ag^0 (Fig. 5B). A continuous decline in the carrier concentration was observed with decreasing the amounts of Ag^0 in $Ag^0:Ag_2Se$. On the contrary, there was a large increase in carrier mobility (Fig. 5B) when more Ag_2Se was present (*i.e.*, less Ag^0 content). The carrier mobility increased from 415.91 $cm^2\ V^{-1}\ s^{-1}$ (45.80% $Ag^0:Ag_2Se$), 908.85 $cm^2\ V^{-1}\ s^{-1}$ (6.10% $Ag^0:Ag_2Se$), 1045.21 $cm^2\ V^{-1}\ s^{-1}$ (4.31% $Ag^0:Ag_2Se$) to 1677.35 $cm^2\ V^{-1}\ s^{-1}$ (1.96% $Ag^0:Ag_2Se$) at 303 K.

The temperature-dependent trends in Seebeck coefficient of $Ag^0:Ag_2Se$ are opposite to those of electrical conductivity and carrier concentration. Greater excessive amounts of Ag^0 from day 1 of the reaction (45.80% $Ag^0:Ag_2Se$) resulted in a significant drop in Seebeck coefficient (Fig. 5C), measured as -35.52 $\mu V\ K^{-1}$ (303 K) and -11.50 $\mu V\ K^{-1}$ (423 K), compared to other samples with lesser amounts of Ag^0. These attributes lead to the lowest power factor for 45.80% $Ag^0:Ag_2Se$ (Fig. 5D), measured as 1.80 mW mK^{-2}, in comparison to 2.14 mW mK^{-2} (6.10% $Ag^0:Ag_2Se$), 2.23 mW mK^{-2} (4.31% $Ag^0:Ag_2Se$), and 2.63 mW mK^{-2} (1.96% $Ag^0:Ag_2Se$) at 303 K.

Finally, the chemical bonding and oxidation states of the Ag 3d state in $Ag^0:Ag_2Se$ with different amounts of Ag^0 (45.80%, 6.10%, 4.31% and 1.96%) were analysed by X-ray photoelectron spectroscopy (XPS) (Fig. S8, ESI†). The two peaks observed in the XPS spectra correspond to Ag $3d_{5/2}$ and Ag $3d_{3/2}$ orbitals from Ag species with a valence of 0 and +1.[33,35] After the reaction for 1 day, the Ag $3d_{5/2}$ and Ag $3d_{3/2}$ binding energies of 45.80% $Ag^0:Ag_2Se$ were measured as 368.6 and 374.6 eV, respectively. After the reaction for 7 days, the Ag $3d_{5/2}$ and Ag $3d_{3/2}$ binding energies of 1.96% $Ag^0:Ag_2Se$ shifted significantly to 368.0 and 374.0 eV (by -0.6 eV). The negative shift in the binding energy of the Ag 3d peak corresponded to the increased amounts of Ag^+ in $Ag^0:Ag_2Se$ (more conversion of Ag^0 to Ag_2Se), due to the greater extent of reaction of Se^0 with small Ag^0 nanoparticles, which was consistent with the observations by XRD (Fig. 1B) and SEM EDX (Fig. S1, ESI†) for the formation of hybridized $Ag^0:Ag_2Se$.

The thermoelectric performances of Ag_2Se and hybridized Ag_2Se with other components (*e.g.*, inorganic particles, carbon-based materials, polymers, *etc.*), prepared by wet chemistry methods in the literature have been summarized in Table S1 (ESI†). It was shown that the maximum thermoelectric *ZT* of 1.96% $Ag^0:Ag_2Se$ pellet reaches 0.89 at room temperature, which is the largest compared to others in the literature. Instead of doping or alloying, our work presents an effective way to organize different nanoscale building blocks by precise hybridization at the nanoscale, preserving the intrinsic properties of Ag_2Se without incorporating different elements. On this basis, it would be of great interest in extending this solution strategy to the synthesis of hybridized multinary silver-based chalcogenides for further enhancing the thermoelectric properties. Additionally, this solution approach could also find uses in the general synthesis of other metal chalcogenides, particularly useful for large-scale production.

3. Conclusions

A facile aqueous solution method has been developed to achieve the composition-tuned hybridization of n-type $Ag^0:Ag_2Se$ under ambient conditions, resulting in hybrids with outstanding thermoelectric properties at room temperature. By prolonging the reaction time, the synthetic process was refined to yield the optimal composition of excessive Ag^0 for enhancement of thermoelectric properties. The stoichiometry of the Ag and Se was controlled by modulating the oxidation states of Ag and Se in the reaction medium, producing a series of $Ag^0:Ag_2Se$ (Ag^0 excess at 50.86%, 45.80%, 15.97%, 6.10%, 4.31% and 1.96%) with new structural control for enhancing and understanding thermoelectric properties. The optimal excessive Ag^0 of 1.96% after 7 days of reaction exhibited a high *ZT* value of close to unity, which is much higher than excessive Ag^0 at 4.31% after 5 days, due to the greatly improved transport properties and Seebeck coefficient. Owing to the superior thermoelectric performance at near room temperature, this hybridization strategy shows great potential to develop new thermoelectric materials for effectively harvesting electricity from low grade heat sources.

4. Experimental section

4.1 Materials

Sodium selenite (Na_2SeO_3, ≥95%), sodium borohydride ($NaBH_4$, 98%) and silver nitrate ($AgNO_3$, ≥99%) were purchased from Sigma-Aldrich. All chemicals were used as received without further purification.

4.2 Synthesis of $Ag^0:Ag_2Se$ hybrids

First, Na_2SeO_3 (40 mmol) was added to water (150 mL) under mild magnetic stirring and continuous argon purging.

Next, $NaBH_4$ (80 mmol) in water (50 mL) was introduced into the solution of Na_2SeO_3 under the protection of argon. The reaction mixture was stirred at room temperature for 6 h until a colourless solution was obtained. Subsequently, $AgNO_3$ (80 mmol) in water (50 mL) was added slowly, forming a black Ag precipitate within 2 minutes of addition (the precipitate was washed immediately in a separate preparation for characterization). Argon purging was then stopped and the solution was stirred continuously for 2 h. The resulting Ag^0 : Ag_2Se precipitates were purified by three rounds of centrifugation/washing with water and then dried in an oven at 60 °C overnight. The above reaction was also repeated with reaction times of 1, 3, 5 and 7 days individually.

4.3 Sample preparation and characterization

Transmission electron microscopy (TEM) images and energy-dispersive X-ray spectroscopy (EDX) mapping were recorded on a JEOL-2100 transmission electron microscope using an acceleration voltage of 200 kV. Scanning electron microscopy (SEM) images (5 kV) and EDX (15 kV) patterns were obtained using a JEOL JSM7600F field-emission scanning electron microscope (FESEM). X-Ray diffraction (XRD) was performed with a D8 Advance X-ray diffractometer operating at 40 kV and 40 mA with Cu Kα radiation (λ = 1.54184 Å). Data were collected from 20 to 60° with a sampling interval of 0.02° per step and a scan speed of 4° per minute. *In situ* XRD was performed with a heating rate at 20 °C min^{-1} from 303 K to 573 K. X-Ray photoelectron spectroscopy (XPS) measurement was performed on a Theta-Probe angle-resolved X-ray photoelectron spectrometer (ARXPS) system (Thermo Scientific) at a base pressure of 1×10^{-9} Torr and a step size of 0.1 eV using monochromated and micro-focused Al Kα X-ray photons ($h\nu$ = 1486.6 eV).

The Ag^0 : Ag_2Se powders were densified using an Elenix high-speed spark plasma sintering (SPS) machine Ed-Pas at 473 K (200 °C) under a pressure of 40 MPa in a graphite die for 10 min. The obtained hot-pressed pellets were cooled to room temperature under vacuum. The Ag^0 : Ag_2Se powders were also densified by a hydraulic press at room temperature for 10 min at a pressure of 10 tons in a stainless-steel die. The cold-pressed pellets were further heat treated at 200 °C for 1 h in a tube furnace under an argon atmosphere.

Their electrical conductivity (σ) and the Seebeck coefficient (S) were measured simultaneously by a standard four-probe method with a ULVAC RIKO ZEM3 system under a helium atmosphere. Their total thermal conductivity (κ) was calculated using the equation $\kappa = a\rho C_p$, in which thermal diffusivity (a) of the pellets was measured using a Netzsch LFA 457 laser flash diffusivity instrument. The hot- and cold-pressed pellets were spray-coated with a thin layer of graphite to minimize radiative heat loss from the material. The specific heat capacity (C_p) was measured using a Mettler Toledo differential scanning calorimeter (DSC) with a heating rate of 2 °C min^{-1}. The density (ρ) of all the pellets was determined to be ≈97% of the theoretical density using the dimension and the mass of the Ag_2Se sample. The Hall coefficient was measured with HMS-5300, ECOPIA with four probes to record the Hall carrier concentration (n_H) and mobility (μ_H) at 303–473 K. The magnetic field size was 0.57 T, and the current strength was set between 10 μA and 20 mA. The transport measurements were repeated three times. The uncertainties are 5% for σ, S, and κ, 10% for PF and ZT.

Author contributions

Conceptualization, data curation, validation, supervision and writing: S. Y. Tee and M. Y. Han. Analysis, investigation, and drafting: D. Ponsford, X. Y. Tan, X. Wang, C. L. Lay, C. J. J. Lee, X. P. Ni, D. H. L. Seng, W. Thitsartarn, and G. Guan.

Conflicts of interest

There are no conflicts to declare.

Acknowledgements

We acknowledge the financial support from the A*STAR SERC MTC YIRG under grant number 21-815515 and A*STAR IMRE-SCG Chemicals Advanced Composite Joint Lab (IAF-ICP) under project number I1801E0024.

References

1 J. He, S. N. Girard, J. C. Zheng, L. Zhao, M. G. Kanatzidis and V. P. Dravid, Strong phonon scattering by layer structured $PbSnS_2$ in PbTe based thermoelectric materials, *Adv. Mater.*, 2012, **24**, 4440–4444.

2 L. D. Zhao, X. Zhang, H. Wu, G. Tan, Y. Pei, Y. Xiao, C. Chang, D. Wu, H. Chi, L. Zheng, S. Gong, C. Uher, J. He and M. G. Kanatzidis, Enhanced Thermoelectric Properties in the Counter-Doped SnTe System with Strained Endotaxial SrTe, *J. Am. Chem. Soc.*, 2016, **138**, 2366–2373.

3 M. Hong, Z. G. Chen, L. Yang, Y. C. Zou, M. S. Dargusch, H. Wang and J. Zou, Realizing zT of 2.3 in $Ge_{1-x-y}Sb_xIn_yTe$ *via* Reducing the Phase-Transition Temperature and Introducing Resonant Energy Doping, *Adv. Mater.*, 2018, **30**, 1705942.

4 C. Forman, I. K. Muritala, R. Pardemann and B. Meyer, Estimating the global waste heat potential, *Renewable Sustainable Energy Rev.*, 2016, **57**, 1568–1579.

5 A. Firth, B. Zhang and A. Yang, Quantification of global waste heat and its environmental effects, *Appl. Energy*, 2019, **235**, 1314–1334.

6 Z. Bu, X. Zhang, Y. Hu, Z. Chen, S. Lin, W. Li, C. Xiao and Y. Pei, A record thermoelectric efficiency in tellurium-free modules for low-grade waste heat recovery, *Nat. Commun.*, 2022, **13**, 237.

7 P. Jood, R. Chetty and M. Ohta, Structural stability enables high thermoelectric performance in room temperature Ag_2Se, *J. Mater. Chem. A*, 2020, **8**, 13024–13037.

8 S. Y. Tee, D. Ponsford, C. L. Lay, X. Wang, X. Wang, D. C. J. Neo, T. Wu, W. Thitsartarn, J. C. C. Yeo, G. Guan,

T. C. Lee and M. Y. Han, Thermoelectric Silver-Based Chalcogenides, *Adv. Sci.*, 2022, **9**, e2204624.

9 W.-Y. Chen, X.-L. Shi, J. Zou and Z.-G. Chen, Thermoelectric coolers for on-chip thermal management: Materials, design, and optimization, *Mater. Sci. Eng. R Rep.*, 2022, **151**, 100700.

10 Q.-X. Hu, W.-D. Liu, L. Zhang, W. Sun, H. Gao, X.-L. Shi, Y.-L. Yang, Q. Liu and Z.-G. Chen, SWCNTs/Ag_2Se film with superior bending resistance and enhanced thermoelectric performance *via* in situ compositing, *Chem. Eng. J.*, 2023, **457**, 141024.

11 T. Cao, X.-L. Shi and Z.-G. Chen, Advances in the design and assembly of flexible thermoelectric device, *Prog. Mater. Sci.*, 2023, **131**, 101003.

12 C. Xiao, J. Xu, K. Li, J. Feng, J. Yang and Y. Xie, Superionic phase transition in silver chalcogenide nanocrystals realizing optimized thermoelectric performance, *J. Am. Chem. Soc.*, 2012, **134**, 4287–4293.

13 A. J. E. Rettie, C. D. Malliakas, A. S. Botana, J. M. Hodges, F. Han, R. Huang, D. Y. Chung and M. G. Kanatzidis, Ag_2Se to KAg_3Se_2: Suppressing Order-Disorder Transitions *via* Reduced Dimensionality, *J. Am. Chem. Soc.*, 2018, **140**, 9193–9202.

14 D. Yang, X. Su, F. Meng, S. Wang, Y. Yan, J. Yang, J. He, Q. Zhang, C. Uher, M. G. Kanatzidis and X. Tang, Facile room temperature solventless synthesis of high thermoelectric performance Ag_2Se *via* a dissociative adsorption reaction, *J. Mater. Chem. A*, 2017, **5**, 23243–23251.

15 J. Chen, Q. Sun, D. Bao, T. Liu, W. D. Liu, C. Liu, J. Tang, D. Zhou, L. Yang and Z. G. Chen, Hierarchical Structures Advance Thermoelectric Properties of Porous n-type beta-Ag_2Se, *ACS Appl. Mater. Interfaces*, 2020, **12**, 51523–51529.

16 J. Chen, H. Yuan, Y. K. Zhu, K. Zheng, Z. H. Ge, J. Tang, D. Zhou, L. Yang and Z. G. Chen, Ternary $Ag_2Se_{1-x}Te_x$: A Near-Room-Temperature Thermoelectric Material with a Potentially High Figure of Merit, *Inorg. Chem.*, 2021, **60**, 14165–14173.

17 J. A. Perez-Taborda, O. Caballero-Calero, L. Vera-Londono, F. Briones and M. Martin-Gonzalez, High Thermoelectric zT in n-Type Silver Selenide films at Room Temperature, *Adv. Energy Mater.*, 2018, **8**, 1702024.

18 X. Zhong, M. Han, Z. Dong, T. J. White and W. Knoll, Composition-tunable $Zn_xCd_{1-x}Se$ nanocrystals with high luminescence and stability, *J. Am. Chem. Soc.*, 2003, **125**, 8589–8594.

19 H. Zhang, K. Cheng, Y. M. Hou, Z. Fang, Z. X. Pan, W. J. Wu, J. L. Hua and X. H. Zhong, Efficient CdSe quantum dot-sensitized solar cells prepared by a postsynthesis assembly approach, *Chem. Commun.*, 2012, **48**, 11235–11237.

20 W. Li, R. Zamani, M. Ibanez, D. Cadavid, A. Shavel, J. R. Morante, J. Arbiol and A. Cabot, Metal ions to control the morphology of semiconductor nanoparticles: copper selenide nanocubes, *J. Am. Chem. Soc.*, 2013, **135**, 4664–4667.

21 R. Xie and M. Zhou, Zinc Chalcogenide Seed-Mediated Synthesis of CdSe Nanocrystals: Nails, Chesses and Tetrahedrons, *Chem. Mater.*, 2015, **27**, 3055–3064.

22 S. Mourdikoudis, M. Menelaou, N. Fiuza-Maneiro, G. Zheng, S. Wei, J. Perez-Juste, L. Polavarapu and Z. Sofer, Oleic acid/oleylamine ligand pair: a versatile combination in the synthesis of colloidal nanoparticles, *Nanoscale Horiz.*, 2022, **7**, 941–1015.

23 W. J. Mir, A. Sharma, D. R. Villalva, J. Liu, M. A. Haque, S. Shikin and D. Baran, The ultralow thermal conductivity and tunable thermoelectric properties of surfactant-free SnSe nanocrystals, *RSC Adv.*, 2021, **11**, 28072–28080.

24 S. Y. Tee, X. Y. Tan, X. Wang, C. J. J. Lee, K. Y. Win, X. P. Ni, S. L. Teo, D. H. L. Seng, Y. Tanaka and M. Y. Han, Aqueous Synthesis, Doping, and Processing of n-Type Ag_2Se for High Thermoelectric Performance at Near-Room-Temperature, *Inorg. Chem.*, 2022, **61**, 6451–6458.

25 Z.-H. Zheng, X.-L. Shi, D.-W. Ao, W.-D. Liu, M. Li, L.-Z. Kou, Y.-X. Chen, F. Li, M. Wei, G.-X. Liang, P. Fan, G. Q. Lu and Z.-G. Chen, Harvesting waste heat with flexible Bi_2Te_3 thermoelectric thin film, *Nat. Sustain*, 2022, **6**, 180–191.

26 P. Vaqueiro, *Inorganic Thermoelectric Materials*, 2021, pp. 1–52, DOI: **10.1039/9781788019590-00001**.

27 H. Wu, J. Carrete, Z. Zhang, Y. Qu, X. Shen, Z. Wang, L.-D. Zhao and J. He, Strong enhancement of phonon scattering through nanoscale grains in lead sulfide thermoelectrics, *NPG Asia Mater.*, 2014, **6**, e108.

28 X. Wang, A. Suwardi, Y. Zheng, H. Zhou, S. W. Chien and J. Xu, Enhanced Thermoelectric Performance of Nanocrystalline Indium Tin Oxide Pellets by Modulating the Density and Nanoporosity *via* Spark Plasma Sintering, *ACS Appl. Nano Mater.*, 2020, **3**, 10156–10165.

29 C. Han, Z. Li, G. Q. Lu and S. Xue Dou, Robust scalable synthesis of surfactant-free thermoelectric metal chalcogenide nanostructures, *Nano Energy*, 2015, **15**, 193–204.

30 K. H. Lim, K. W. Wong, Y. Liu, Y. Zhang, D. Cadavid, A. Cabot and K. M. Ng, Critical role of nanoinclusions in silver selenide nanocomposites as a promising room temperature thermoelectric material, *J. Mater. Chem. C*, 2019, **7**, 2646–2652.

31 H. Wang, W. Chu, D. Wang, W. Mao, W. Pan, Y. Guo, Y. Xiong and H. Jin, Low-Temperature Thermoelectric Properties of β-Ag_2Se Synthesized by Hydrothermal Reaction, *J. Electron. Mater.*, 2011, **40**, 624–628.

32 D. Li, J. H. Zhang, J. M. Li, J. Zhang and X. Y. Qin, High thermoelectric performance for an Ag_2Se-based material prepared by a wet chemical method, *Mater. Chem. Front.*, 2020, **4**, 875–880.

33 Y. Lu, Y. Qiu, K. Cai, Y. Ding, M. Wang, C. Jiang, Q. Yao, C. Huang, L. Chen and J. He, Ultrahigh power factor and flexible silver selenide-based composite film for thermoelectric devices, *Energy Environ. Sci.*, 2020, **13**, 1240–1249.

34 J. Gao, L. Miao, H. Lai, S. Zhu, Y. Peng, X. Wang, K. Koumoto and H. Cai, Thermoelectric Flexible Silver Selenide Films: Compositional and Length Optimization, *iScience*, 2020, **23**, 100753.

35 X. Li, Y. Lu, K. Cai, M. Gao, Y. Li, Z. Wang, M. Wu, P. Wei, W. Zhao, Y. Du and S. Shen, Exceptional power factor of flexible Ag/Ag_2Se thermoelectric composite films, *Chem. Eng. J.*, 2022, **434**, 134739.